

Entanglement, excitations and correlation effects in narrow zigzag graphene nanoribbons

I. Hagymási and Ö. Legeza

*Strongly Correlated Systems "Lendület" Research Group, Institute for Solid State Physics and Optics,
MTA Wigner Research Centre for Physics, Budapest H-1525 P.O. Box 49, Hungary*

We investigate the low-lying excitation spectrum and ground-state properties of narrow graphene nanoribbons with zigzag edge configurations. Nanoribbons of comparable widths have been synthesized very recently [P. Ruffieux, *et al.* Nature **531**, 489 (2016)], and their descriptions require more sophisticated methods since in this regime conventional methods, like mean-field or density-functional theory with local density approximation, fail to capture the enhanced quantum fluctuations. Using the unbiased density-matrix renormalization group algorithm we calculate the charge gaps with high accuracy for different widths and interaction strengths and compare them with mean-field results. It turns out that the gaps are much smaller in the former case due to the proper treatment of quantum fluctuations. Applying the elements of quantum information theory we also reveal the entanglement structure inside a ribbon and examine the spectrum of subsystem density matrices to understand the origin of entanglement. We examine the possibility of magnetic ordering and the effect of magnetic field. Our findings are relevant for understanding the gap values in different recent experiments and the deviations between them.

PACS numbers: 71.10.Fd, 71.10.Hf, 73.22.-f

I. INTRODUCTION

Graphene, the two-dimensional honeycomb lattice of carbon atoms has attracted an enormous interest since its first discovery in 2004.¹ In spite of this, from the point of view of applications in nanoelectronics, bulk graphene is not useful due to the absence of a band gap. Therefore, finite samples of graphene are likely to be more advantageous in this aspect, since they may exhibit a gap due to quantum confinement or electronic correlations. Graphene nanoribbons are especially promising candidates in overcoming this obstacle. It has been demonstrated, that nanoribbons with a well-defined crystallographic orientation can be produced with scanning-tunneling-microscope-based lithography^{2,3} and even sub 4 nm widths can be achieved. On the other hand bottom-up techniques now make it possible to synthesize either armchair⁴ or zigzag⁵ nanoribbons whose widths consist of a few zigzag carbon lines only. Ribbons with a zigzag edge are particularly interesting because of their peculiar electronic and magnetic properties.^{6,7} While a graphene sheet can be considered as a marginal Fermi liquid,⁸ and can be treated practically as a non-interacting system, the situation is completely different for nanoribbons with a zigzag edge. It is known from conventional band theory that these ribbons have a flat band due to their edge states.⁶ This large density of states at the Fermi energy is very sensitive to magnetic ordering, even if only a weak electron-electron interaction is present based on the the Slater theory of antiferromagnetism. Note that such a drastic effect does not occur in armchair ribbons due to the absent edge states, therefore we focus on zigzag ribbons in the following. As a result of the interaction, a gap opens in zigzag ribbons, which implies magnetically ordered edge states as it has been demonstrated in an indirect way recently with the contribution of one of us.³

The above facts motivated the exploration of the interaction effects with the use of several methods, like density-functional theory (DFT),^{7,9-12} mean-field approximation,¹³⁻²⁰ quantum Monte Carlo (QMC)²¹⁻²³ and density-matrix renormalization group algorithm (DMRG).²⁴⁻²⁶ The DFT and DMRG in Ref. [25] are used in ab-initio calculations, while the other methods are applied in solving the π -band model of graphene, that is, the Hubbard model on a honeycomb ribbon:

$$\mathcal{H} = \sum_{ij} t_{ij} \hat{c}_i^\dagger \hat{c}_j + U \sum_i \hat{n}_{i\uparrow} \hat{n}_{i\downarrow}, \quad (1)$$

where t_{ij} is the hopping amplitude between sites i and j , and U is the strength of the local Coulomb interaction. In what follows we consider only nearest-neighbor hopping terms, with $t = 2.7$ eV. The most extensive studies were performed with DFT and in mean-field approximation because broad ribbons can easily be accessed, while alternative approaches have been suggested recently to treat large system sizes.²⁷ Density functional and mean-field theories reduce the original interacting system to an effective single-particle problem, therefore they neglect correlation effects and quantum fluctuations which are known to be significant in quasi one-dimensional systems. For this reason a more accurate description is necessary, which QMC and DMRG are able to address. Due to the exponential growth of the Hilbert space, these methods can treat only much smaller sizes. The QMC studies mainly focused on the correlation between edge atoms and dynamical properties,²² and the previous DMRG model calculations were restricted to very small systems.^{24,26} In the widespread use of mean-field theory, it is important to investigate its reliability by examining the role of enhanced quantum fluctuations, which this approximation neglects. Although a benchmark of mean-field theory was performed for quantum

dot-like structures,²¹ less is known about the case of zigzag nanoribbons. It has been shown previously that QMC results agree well quantitatively with mean-field results for wide enough ribbons in the weakly interacting limit.²² In light of the new fact that zigzag ribbons with already five zigzag carbon lines width can be created,⁵ it is necessary to analyze such narrow ribbons where dimensionality effects are expected to be more crucial. Here we intend to fill a major gap with the DMRG method by investigating the low-lying energy spectrum of zigzag ribbons in a controlled, accurate manner. We calculate the charge gaps for various interaction strengths and compare them with the mean-field results. Moreover, they are also experimentally relevant quantities, since they can be accessed by scanning tunneling microscopy measurements.³ Furthermore, we address the ground-state properties by considering not only the correlations between the edge atoms, but between every pair of sites, which provides us a deeper insight into the many-body aspect of the graphene nanoribbons. We also investigate the magnetic properties of the ground state and the effect of external magnetic field.

The paper is organized as follows. Section II. contains the numerical details of the DMRG method. In Section III. A we present our results for the charge gaps for various ribbon widths and interaction strengths and compare them with the mean-field results. Section III. B demonstrates the application of quantum information theory in determining the entanglement patterns and correlation functions of nanoribbons. In Section III. C the magnetic properties are addressed. In Section III. D we discuss how our results for the charge gap are related to recent experiments and DFT calculations. Finally, in Section IV. our conclusions are presented.

II. METHODS

We apply the DMRG algorithm in real space²⁸⁻³³ and use the dynamic block-state selection approach (DBSS),^{34,35} which enables us the accurate control of the truncation error. In our case, the a priori value of the quantum information loss was set to $\chi = 10^{-4}$ and the truncation errors were in the order of 10^{-6} . This threshold value required block states about 15000-20000 so that, our results are far more accurate than those from previous investigations,²⁴⁻²⁶ in terms of the truncation procedure. Such a large number of block states is necessary to obtain accurate gap values and correlation functions. We considered ribbons with a maximum number of sites $L = 84$ and open boundary condition is applied at every edge. A honeycomb ribbon is mapped to a one-dimensional chain, with long-range hopping elements. The ordering of the sites and the geometry of the ribbon is given in Fig. 1.

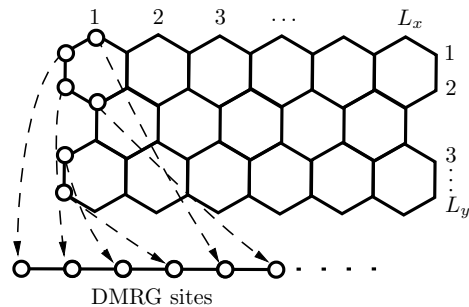


FIG. 1. The applied notations for the length and width of a zigzag ribbon, and the mapping used in the DMRG calculation.

III. RESULTS

A. Charge gap

In what follows we restrict ourselves to half-filled case. We know that in this case Lieb's theorem³⁶ forbids the appearance of spontaneous spin polarization, however, the low-lying spectrum can be obtained. In fact, with scanning tunneling microscopy one can measure the band gap, which in our case corresponds to the single-particle excitation, usually referred as the charge gap:

$$\Delta(L) = \frac{1}{2} \left[E_0 \left(\frac{L}{2} + 1, \frac{L}{2} \right) + E_0 \left(\frac{L}{2} - 1, \frac{L}{2} \right) - 2E_0 \left(\frac{L}{2}, \frac{L}{2} \right) \right], \quad (2)$$

where $E_0(N_\uparrow, N_\downarrow)$ is the ground state in sector with N_\uparrow up-spin and N_\downarrow down-spin electrons and $L = 2L_xL_y + L_y$ is the total number of sites. We calculated the charge gaps for different values of U and two different widths, $L_y = 2$ and 4. The maximum length we could achieve was $L_x = 10$ for $L_y = 4$. The Hubbard U was varied within the range $U/t = 0$ and 4, since around $U_c/t \sim 3.9$ a Mott-transition occurs in the two-dimensional honeycomb lattice,³⁷⁻³⁹ and larger values are not physical in case of graphene. A careful extrapolation of the gaps to the thermodynamic limit was performed in each case as it is demonstrated in Fig. 2 for $L_y = 4$. The data for $L_y = 4$ were fitted using an exponential function:

$$\Delta(L_x) = \Delta(\infty) + A \exp(-B/L_x), \quad (3)$$

with $\Delta(\infty)$, A and B being free parameters. For $L_y = 2$ we obtained the same results as in Ref. [24] (see Fig. 3), where the finite-size scaling of the gaps can be fitted with a quadratic function, which may be due to the stronger one-dimensional effects. In this case a much smaller number of block states, ~ 500 , was sufficient to keep the truncation errors in the order of 10^{-6} . However, for $L_y = 4$ 15000-20000 block states are necessary to obtain energy values within the same error margin. Since the ground-state energies are in the order of $\sim 10^2$ and the magnitude

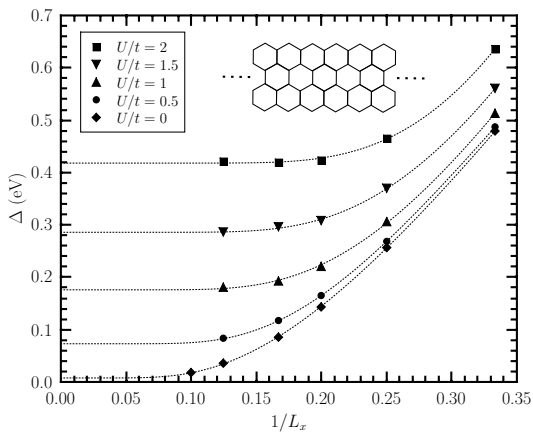


FIG. 2. Finite-size scaling of charge gaps for different values of U and $L_y = 4$ as indicated by the inset figure. The dotted lines denote the exponential fit to the data described in the main text.

of the truncation errors is $\sim 10^{-6}$, we estimate that the error of the gaps is around $\sim 10^{-4}$, which is much smaller than the size of the symbols in Fig. 2. The extrapolated gap values as a function of U are shown in Fig. 3 for two different widths. Our results suggest that the charge

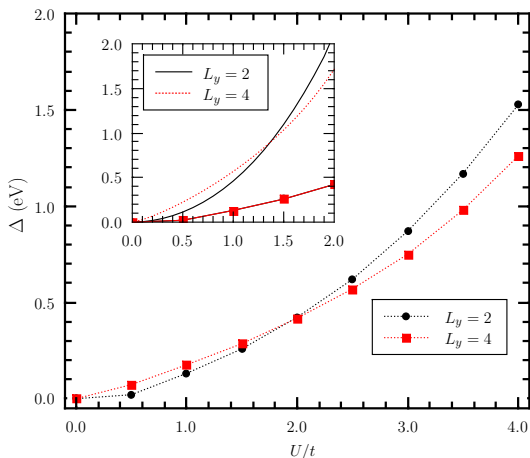


FIG. 3. (color online) DMRG results for the charge gaps as a function of U for two different widths ($L_y = 2$ and 4) as indicated in the legend. The dotted lines are guides to the eye. The inset shows the bandgaps obtained with the mean-field approximation of the Hubbard-model (solid and dotted lines) together with the DMRG data.

gap opens at $U/t = 0$, which might be the residue of the Slater transition occurring in the mean-field treatment. This is also in agreement with the previous prediction²⁴ based on the analysis of narrower ribbons. It is worth comparing these results to those obtained from mean-field theory whose details have been described in several papers.^{15,21} We performed mean-field calculations for the present ribbons (see Appendix for the details), and the obtained mean-field gaps are shown in the inset of Fig. 3. They exhibit qualitatively very similar behavior, how-

ever, they are remarkably larger than the DMRG gap values. This can be attributed to the neglect of quantum fluctuations, which are enhanced at such narrow widths. It is worth mentioning that for small two-dimensional structures, the mean-field theory provided quite accurate results in comparison with QMC.²¹ This may follow from the fact that the quantum fluctuations in a two-dimensional systems are not as strong as in one dimension.

B. Quantum information analysis, correlation functions

As a next step we consider the ground-state properties by investigating various correlation functions. Our aim is to investigate the correlations between two given subsystems, namely, between two sites. The knowledge of this quantity provides information about the whole system. This can be obtained from the mutual information:^{40–42}

$$I_{ij} = s_i + s_j - s_{ij}, \quad (4)$$

which measures all types of correlations (both of classical and quantum origin) between sites i and j , we will refer to this quantity as the strength of entanglement between the system components. Here s_i and s_{ij} are the one- and two-site von Neumann entropies,^{43–48} respectively, that can be calculated from the corresponding reduced density matrices:

$$s_i = -\text{Tr} \rho_i \ln \rho_i, \quad (5)$$

$$s_{ij} = -\text{Tr} \rho_{ij} \ln \rho_{ij}, \quad (6)$$

where ρ_i (ρ_{ij}) is the reduced density matrix of site i (sites i and j), which is derived from the density matrix of the total system by tracing out the configurations of all other sites. In this part, we calculate the mutual information for different values of the Hubbard interaction to reveal how the interaction modifies the original ground state.

We use the sum of one-site entropies,⁴⁹ I_{TOT} , and the entanglement distance,⁴⁷ $I_{\text{dist}}^{(\text{MPS}/\text{real}),\eta}$:

$$I_{\text{TOT}} = \sum_i s_i, \quad (7)$$

$$I_{\text{dist}}^{(\text{MPS}/\text{real}),\eta} = \sum_{ij} I_{ij} \left(d_{ij}^{(\text{MPS}/\text{real})} \right)^\eta, \quad (8)$$

where $d_{ij}^{(\text{MPS})} = |i - j|$ is for the one-dimensional topology of the DMRG and $d_{ij}^{(\text{real})}$ is the distance in physical lattice space. I_{TOT} and $I_{\text{dist}}^{(\text{MPS}/\text{real}),\eta}$ quantify the total quantum information encoded in the wave function and the localization of entanglement in the system, respectively. Firstly, we consider the noninteracting case. The entanglement patterns obtained from the mutual information are shown in Fig. 4 for a system with $L_x = 6$ and $L_y = 4$. It is clearly observed, that mainly short-range correlations are present, and certain opposite sites

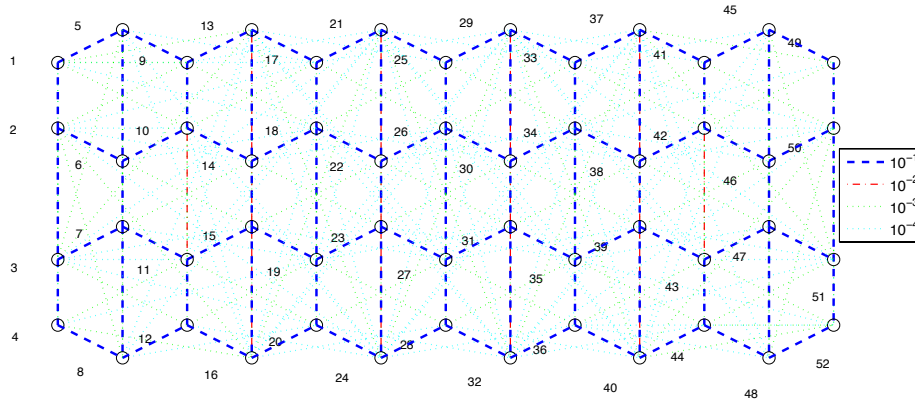


FIG. 4. (color online) Entanglement patterns in a zigzag ribbon for $L_x = 6$, $L_y = 4$ and $U = 0$. The various types of lines correspond to different magnitudes as indicated in the sidebar. The numbers indicate the positions of sites along the one-dimensional DMRG topology. The blue dashed lines connect only nearest-neighbor sites (for example: sites $i = 1, 2$ or $i = 1, 5$), or opposite sites within a hexagon (for example: sites $i = 9, 10$ or $i = 22, 23$). The red dash-dot lines connect opposite zigzag sites, for example: $i = 13, 16$.

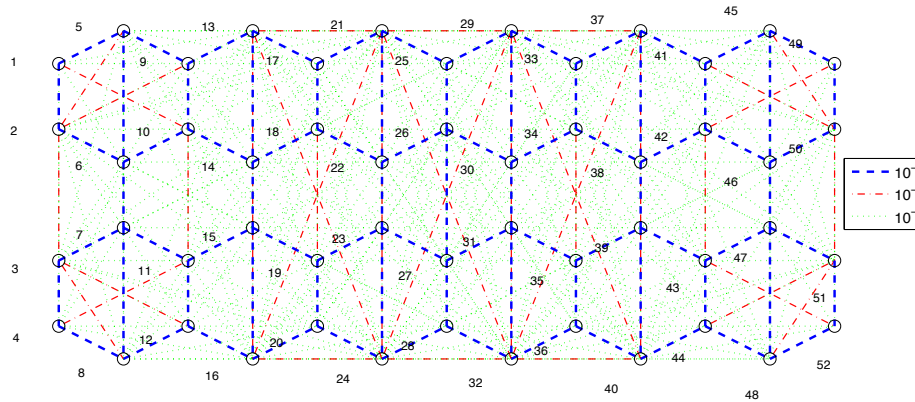


FIG. 5. (color online) Similar to Fig. 4 but for $U/t = 2$, furthermore the red dash-dot lines at the zigzag edges connect neighboring zigzag sites, for example: $i = 13, 21$ or $i = 24, 32$.

in a hexagon are entangled, but there is no strong entanglement between the two edges (note that red and green lines correspond to one and two orders of magnitude smaller values, respectively). In this case a maximum number of block states ~ 8000 was sufficient to determine the ground state wave function within our error margin. As a next step, we investigate what happens when the electrons are interacting. To emphasize the interaction effects, we set $U/t = 2$. The results are shown in Fig. 5. It is remarkable, that besides the strong nearest-neighbor entanglement, moderately strong entanglement appears between the two edges, and between electrons on the same edge. It is interesting to mention that here a maximum number of ~ 15000 block states was necessary to obtain the ground state, which is almost twice as large as in the noninteracting case using the same threshold value in the truncation procedure. In agree-

ment with this $I_{\text{dist}}^{(\text{MPS}),2}(U = 0) = 232.07$ increases to $I_{\text{dist}}^{(\text{MPS}),2}(U = 2t) = 371.12$ and similarly $I_{\text{dist}}^{(\text{real}),2}(U = 0) = 38.67$ increases to $I_{\text{dist}}^{(\text{real}),2}(U = 2t) = 51.27$. Therefore, for $U/t = 2$ longer range entanglement bonds appear, as indicated by $I_{\text{dist}}^{(\text{real}),2}$, in contrast to the $U = 0$ case, whose presence naturally requires much larger bond dimensions since these entanglement bonds are cut when subsystem entropies are calculated. The sum of one-site entropies decreases with U ($I_{\text{TOT}}(U = 0) = 72.08$, $I_{\text{TOT}}(U = 2t) = 70.45$), but in a much lower rate than in the one-dimensional case. We also mention that the ground states in both cases are spin singlets, and finite spin polarization does not appear at the edges, since the ground state respects the rotational symmetry of the original Hamiltonian, in agreement with the previous DMRG and QMC results. This is in sharp contrast with

the mean-field results, where a broken-symmetry ground state is realized and the ferromagnetically polarized edges are coupled to each other antiferromagnetically.

The analysis so far has given us an overall picture about which sites are strongly entangled, but to obtain additional information about the nature of the entanglement it is worth investigating the eigensystem of the two-site density matrices. Firstly, we consider two neighboring zigzag sites, (24 and 32 in Fig. 5) and solve the eigenvalue problem of the corresponding two-site reduced density matrix, $\rho_{24,32}$. In its eigenvalue spectrum, the most significant eigenvalue ($\omega = 0.128$) is threefold degenerate, and the corresponding eigenvectors are:

$$\begin{aligned}\phi_{24,32}^{(1)} &= |\uparrow\rangle_{24}|\uparrow\rangle_{32}, \\ \phi_{24,32}^{(2)} &= \frac{1}{\sqrt{2}}(|\uparrow\rangle_{24}|\downarrow\rangle_{32} + |\downarrow\rangle_{24}|\uparrow\rangle_{32}), \\ \phi_{24,32}^{(3)} &= |\downarrow\rangle_{24}|\downarrow\rangle_{32}.\end{aligned}\quad (9)$$

It means that in this mixed state the largest weight belongs to the triplet components, which results in a ferromagnetic correlation between the two neighboring zigzag sites. Similarly, we investigate the reduced density matrix of two zigzag sites sitting on opposite edges, e.g. 29 and 32. Performing the same analysis, we find that the eigenvector corresponding to the largest eigenvalue ($\omega = 0.19$) is:

$$\begin{aligned}\phi_{29,32} &= \\ &0.7067(|\uparrow\rangle_{29}|\downarrow\rangle_{32} - |\downarrow\rangle_{29}|\uparrow\rangle_{32}) \\ &+ 0.0236(|\uparrow\downarrow\rangle_{29}|0\rangle_{32} + |0\rangle_{29}|\uparrow\downarrow\rangle_{32}),\end{aligned}\quad (10)$$

which describes that the two electrons on the opposite edges form a singlet. This can be considered as a direct evidence for the antiferromagnetic coupling between the two edges mediated by the conduction electrons in the ribbon.

The above statements have been obtained for a finite length, thus it is important to investigate their size-dependence, which is shown in Fig. 6. Here one can see the spin correlations ($\langle \mathbf{S}_i \mathbf{S}_j \rangle$) between the opposite edges and between neighboring edge atoms as a function of inverse ribbon length taken at the middle of the ribbon. In the case of odd L_x values we performed an average over the two correlation values in the middle of the ribbon to reduce the oscillation due to the finite-size effects. It is easily seen that the absolute value of both quantities increases with the ribbon length, confirming that the above results remain valid even in the thermodynamic limit.

C. Magnetic properties

Previously we revealed the behavior of correlation functions inside the ribbon. Naturally, we did not find long-range magnetic order in finite-systems due to the SU(2) symmetry of the Hamiltonian. However, this

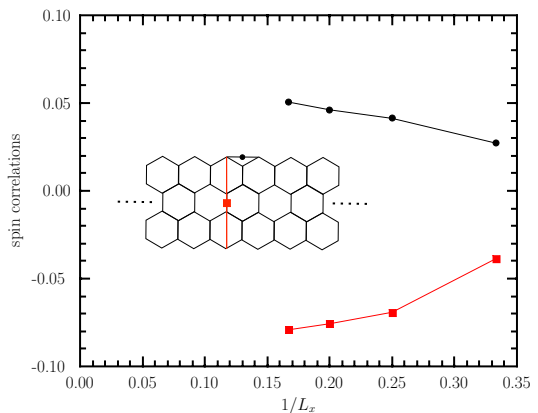


FIG. 6. (color online) Finite-size scaling of spin correlations between the opposite edges (red squares) and between neighboring edge atoms for $U/t = 2$ (black circles), calculated in the middle of the ribbon as they are indicated in the inset figure.

may not be true in the thermodynamic limit, where symmetry-breaking ground state can occur.²³ We investigate this aspect, by adding an artificial pinning magnetic field along the z -direction at the bottom sites of the ribbon to the Hamiltonian (1):

$$\mathcal{H}_{\text{pin}} = -h \sum_i' S_i^z, \quad (11)$$

where the prime denotes that the summation is over only the bottom sites of the ribbon (for example sites 8,16,24,... in Fig. 4). We apply a tiny magnetic field, $h = 0.01t$, to explore possible magnetic order by investigating the response of the system for various values of the Hubbard interaction. The results are shown in Figs. 7 (a)-(c). One can clearly see in Fig. 7 (a) that for $U/t = 0$ the pinning magnetic field hardly triggers any magnetic moment, as it is expected for a paramagnetic ground state. The situation is quite different as U is switched on. For $U/t = 2$ remarkable spin polarization appears at the edges, $S_i^z \sim 0.06$, while much smaller magnetic moments appear inside the ribbon. This corresponds to the regime where the edge magnetism is expected to occur. Increasing U near the critical U_c , significant spin polarization appears also inside the ribbon, whose magnitude is comparable to the magnetic moments at the edges. This reflects the tendency that the honeycomb lattice becomes antiferromagnetically ordered above the critical value. However, here a crossover takes place since the charge gap opens up for any $U/t > 0$ in the zigzag ribbon unlike in the fully two-dimensional honeycomb lattice, where the Mott transition occurs at a finite U_c .

As a next step we investigate what happens if a uniform external magnetic field is applied. To address this question we consider the first spin excited state of the Hamiltonian (1), with $S_{\text{TOT}}^z = 1$, $S = 1$ quantum numbers. The results are shown in Figs. 7 (d)-(f). Qualitatively similar behavior is observed in the bulk as in the

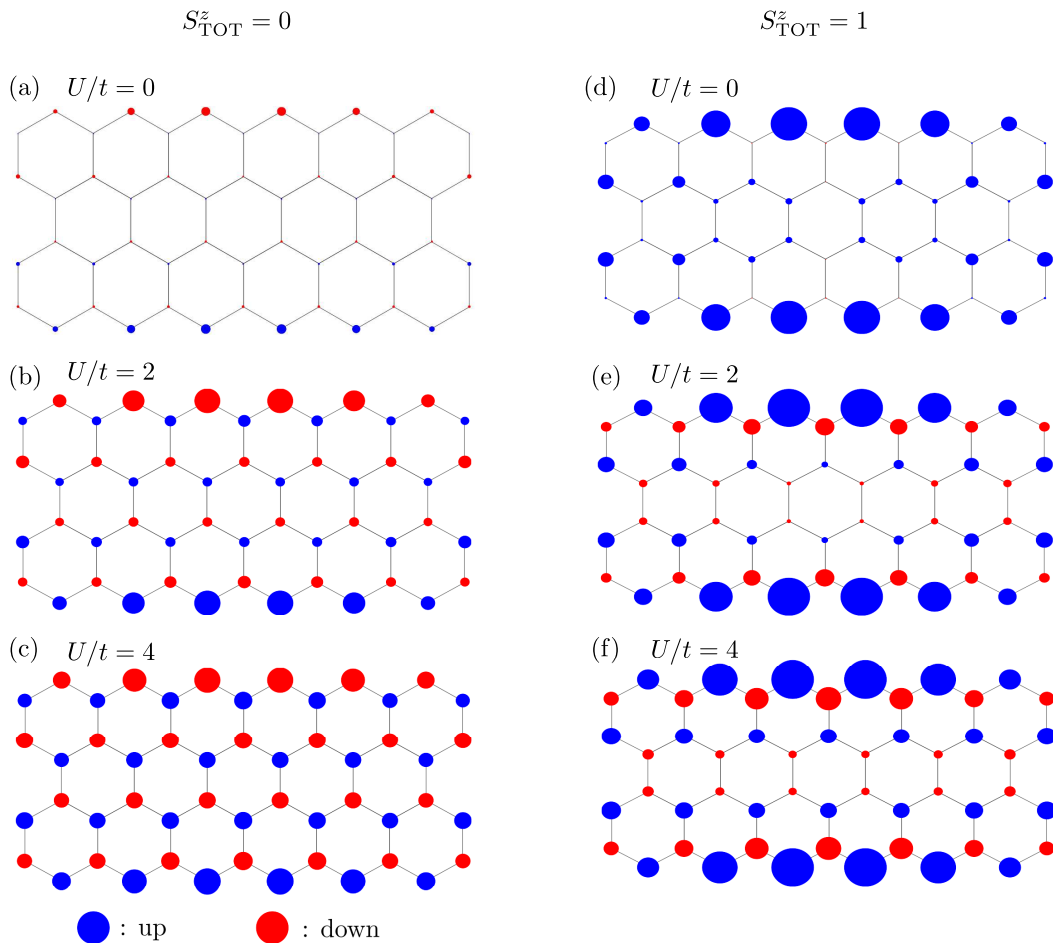


FIG. 7. (color online) Panels (a)-(c) show the local magnetic moments (S_i^z) of the ground state in the presence of a pinning magnetic field at the bottom zigzag sites, $h/t = 0.01$, for various values of U . Panels (d)-(f) show the distribution of local magnetic moments in the $S_{TOT}^z = 1$, $S = 1$ sector for different values of U . The magnitude of up and down moments are proportional to the area of the circles.

previous case, however, the polarization of the edges is more robust in all cases, even for $U/t = 4$. This substantiates the findings of Ref. [24] that the zigzag sites at the edges can be polarized in the easiest way.

D. Discussion

We discuss our results in the light of recent experiments⁵ where ribbons with a comparable width were investigated. To account for the reported gaps of $\Delta_{\text{exp}} \sim 1.5$ eV, the Hubbard- U should be tuned very close to the Mott-insulating regime, see Fig. 3. This may not be a surprise for us since in free-standing graphene the Hubbard- U was estimated $U/t \sim 3.4$,⁵⁰ which is quite close to U_c . Larger values of U are not reasonable in our case, since the bulk graphene is not an insulator. Note that the gaps may be further increased by the inclusion of longer-range interactions, since the screening may not be as effective as in ordinary metals. This hypothesis is corroborated by DFT+ GW calculations,^{9,51} where a sig-

nificant increase of the gaps has been observed compared with what has been obtained in local-density approximation (LDA).⁷ It is also in agreement with the fact that the scanning-tunneling-microscope measurements were carried out in such an environment where the sample was embedded on an insulator.⁵ Here one can expect that the on-site Coulomb interaction is close to the value of the free-standing graphene and long-range interaction might be important. Thus, as we have seen $U/t \sim 3.4 - 3.9$ results in gaps lying very close the experimental values. On the other hand, when the ribbon is placed on the top of a metal host,³ the experimental gap values, $\Delta_{\text{exp}} \sim 0.3$ eV, are smaller by almost an order of magnitude. This can be explained, if we recall that in this case the host metal induces extra charge carriers into the ribbon – indicated by the presence of a finite density of states at the Fermi energy –, therefore the screening of the Coulomb interaction is stronger. Hence, the π -band model containing a much weaker Hubbard interaction term, $U/t \sim 1.5$, than in the free-standing case, provides quantitatively accurate gap values in this case. Another possible importance of our

results is the fact that the gap values cannot be increased above $\Delta \sim 0.3\text{-}0.4$ eV by creating narrower and narrower ribbons – in contrast to prediction of the naive mean-field theory –, as long as the ribbon can be described by the conventional π -band model, like in the experimental setup of Ref. [3]. Furthermore, we emphasize that the widely used mean-field approach cannot be applied even for wider ribbons for $U/t \gtrsim 2.23$, since this theory predicts a Mott-insulating state in the honeycomb lattice above this value,⁵² which turned out to be inaccurate by more sophisticated calculations.³⁷⁻³⁹

IV. CONCLUSIONS

In this paper we examined the charge gaps and ground-state properties of narrow zigzag graphene nanoribbons by applying the unbiased DMRG method with high accuracy to the π -band model containing only local interaction terms. It turned out that the mean-field theory grossly overestimates the gap values in the case of such narrow widths. This discrepancy can be ascribed to the fact that the enhanced quantum fluctuations suppress their values. Our analysis also revealed how the deviations between recent experiments can be understood in terms of the π -band model with a local Coulomb interaction. It was argued that depending on the effectiveness of screening, tuning the value of the on-site Hubbard term, the model can account for quantitatively accurate gap values. We performed a quantum information analysis and determined the spectrum of subsystem density matrices and the entanglement patterns in the ribbons, which gave us a spectacular description of the many-body aspect of the ground states. We pointed out how the entanglement evolves as the interaction is switched on. The understanding of the entanglement structure in nanoribbons is important from the point of view of their future applications in quantum information processing or quantum computation. Finally, we investigated the magnetic properties of nanoribbons and explored possible magnetic orders for various values of the Hubbard interaction.

ACKNOWLEDGMENTS

We acknowledge helpful discussions with F. Gebhard, L. Tapasztó and P. Vancsó. This work was supported in part by the Hungarian Research Fund (OTKA) through Grant Nos. K120569 and NN110360.

Appendix: Details of the mean-field calculation

We performed mean-field calculations to benchmark its gap values against the DMRG results. Using the standard procedure for the decoupling of the Hubbard term we arrive at

$$\mathcal{H}' = -t \sum_{\langle ij \rangle \sigma} (\hat{c}_{i\sigma}^\dagger \hat{c}_{j\sigma} + \text{H.c.}) + U \sum_i (\hat{n}_{i\uparrow} \langle \hat{n}_{i\downarrow} \rangle + \hat{n}_{i\downarrow} \langle \hat{n}_{i\uparrow} \rangle - \langle \hat{n}_{i\downarrow} \rangle \langle \hat{n}_{i\uparrow} \rangle), \quad (\text{A.1})$$

where we have made use of the fact that only nearest-neighbor hoppings are allowed and the summation in the first term is carried out for nearest-neighbor sites. Since we deal with a single-particle problem, the Hamiltonian can be diagonalized by a Bogoliubov transformation in k -space:

$$\mathcal{H}' = \sum_{k\sigma n} \varepsilon_{nk\sigma} \hat{C}_{nk\sigma}^\dagger \hat{C}_{nk\sigma} - U \sum_i \langle \hat{n}_{i\uparrow} \rangle \langle \hat{n}_{i\downarrow} \rangle, \quad (\text{A.2})$$

where $\hat{C}_{nk\sigma}^\dagger$ ($\hat{C}_{nk\sigma}$) are the transformed operators that destroy (create) a particle with wavenumber k with spin σ in band n . The energy bands are given by $\varepsilon_{nk\sigma}$ which depend on the yet unknown electron densities. The densities and energy bands are calculated selfconsistently. For a given ribbon width, L_y , we obtain $2L_y$ bands according to the number of sites in the unit cell of the ribbon. Since we deal with the half-filled case, the first L_y bands are completely filled, thus, the energy gap is determined as the bandgap between bands $n = L_y$ and $n = L_y + 1$. This is shown in the inset of Fig. 3.

¹ K. S. Novoselov, A. K. Geim, S. V. Morozov, D. Jiang, Y. Zhang, S. V. Dubonos, I. V. Grigorieva, and A. A. Firsov, *Science* **306**, 666 (2004).
² L. Tapasztó, G. Dobrik, P. Lambin, and L. P. Biró, *Nat. Nano.* **3**, 397 (2008).
³ G. Z. Magda, X. Jin, I. Hagymási, P. Vancsó, Z. Osváth, P. Nemes-Incze, C. Hwang, L. P. Biró, and L. Tapasztó, *Nature* **514**, 608 (2014).
⁴ A. Kimouche, M. M. Ervasti, R. Drost, S. Halonen, A. Harju, P. M. Joensuu, J. Sainio, and P. Liljeroth, *Nat. Commun.* **6**, 10177 (2015).
⁵ P. Ruffieux, S. Wang, B. Yang, C. Sánchez-Sánchez, J. Liu, T. Dienel, L. Talirz, P. Shinde, C. A. Pignedoli, D. Passerone, T. Dumslaff, X. Feng, K. Müllen, and

R. Fasel, *Nature* **531**, 489 (2016).
⁶ M. Fujita, K. Wakabayashi, K. Nakada, and K. Kusakabe, *J. Phys. Soc. Jpn.* **65**, 1920 (1996).
⁷ Y.-W. Son, M. L. Cohen, and S. G. Louie, *Phys. Rev. Lett.* **97**, 216803 (2006).
⁸ J. González, F. Guinea, and M. A. H. Vozmediano, *Phys. Rev. B* **59**, R2474 (1999).
⁹ L. Yang, C.-H. Park, Y.-W. Son, M. L. Cohen, and S. G. Louie, *Phys. Rev. Lett.* **99**, 186801 (2007).
¹⁰ T. Wassmann, A. P. Seitsonen, A. M. Saitta, M. Lazzeri, and F. Mauri, *Phys. Rev. Lett.* **101**, 096402 (2008).
¹¹ O. V. Yazyev and M. I. Katsnelson, *Phys. Rev. Lett.* **100**, 047209 (2008).

- ¹² Y. Li, Z. Zhou, C. R. Cabrera, and Z. Chen, *Sci. Rep.* **3**, 2030 (2013).
- ¹³ J. Fernández-Rossier, *Phys. Rev. B* **77**, 075430 (2008).
- ¹⁴ O. V. Yazyev, *Phys. Rev. Lett.* **101**, 037203 (2008).
- ¹⁵ J. Jung and A. H. MacDonald, *Phys. Rev. B* **79**, 235433 (2009).
- ¹⁶ S.-T. Pi, K.-P. Dou, C.-S. Tang, and C.-C. Kaun, *Carbon* **94**, 196 (2015).
- ¹⁷ J. Jung, *Phys. Rev. B* **83**, 165415 (2011).
- ¹⁸ J. Jung, T. Pereg-Barnea, and A. H. MacDonald, *Phys. Rev. Lett.* **102**, 227205 (2009).
- ¹⁹ H. Kumazaki and D. S. Hirashima, *J. Phys. Soc. Jpn.* **77**, 044705 (2008).
- ²⁰ A. R. Carvalho, J. H. Warnes, and C. H. Lewenkopf, *Phys. Rev. B* **89**, 245444 (2014).
- ²¹ H. Feldner, Z. Y. Meng, A. Honecker, D. Cabra, S. Wessel, and F. F. Assaad, *Phys. Rev. B* **81**, 115416 (2010).
- ²² H. Feldner, Z. Y. Meng, T. C. Lang, F. F. Assaad, S. Wessel, and A. Honecker, *Phys. Rev. Lett.* **106**, 226401 (2011).
- ²³ M. Golor, S. Wessel, and M. J. Schmidt, *Phys. Rev. Lett.* **112**, 046601 (2014).
- ²⁴ T. Hikihara, X. Hu, H.-H. Lin, and C.-Y. Mou, *Phys. Rev. B* **68**, 035432 (2003).
- ²⁵ W. Mizukami, Y. Kurashige, and T. Yanai, *J. Chem. Theor. and Comp.* **9**, 401 (2013), pMID: 26589042.
- ²⁶ V. M. L. D. P. Goli, S. Prodhon, S. Mazumdar, and S. Ramasesha, *Phys. Rev. B* **94**, 035139 (2016).
- ²⁷ C. Koop and M. J. Schmidt, *Phys. Rev. B* **92**, 125416 (2015).
- ²⁸ S. R. White, *Phys. Rev. Lett.* **69**, 2863 (1992).
- ²⁹ S. R. White, *Phys. Rev. B* **48**, 10345 (1993).
- ³⁰ U. Schollwöck, *Rev. Mod. Phys.* **77**, 259 (2005).
- ³¹ R. M. Noack and S. Manmana, *AIP Conf. Proc.* **789**, 93 (2005).
- ³² K. Hallberg, *Adv. Phys.* **55**, 477 (2006).
- ³³ S. Szalay, M. Pfeffer, V. Murg, G. Barcza, F. Verstraete, R. Schneider, and Ö. Legeza, *Int. J. Quant. Chem.* **115**, 1342 (2015).
- ³⁴ Ö. Legeza, J. Röder, and B. A. Hess, *Phys. Rev. B* **67**, 125114 (2003).
- ³⁵ Ö. Legeza and J. Sólyom, *Phys. Rev. B* **70**, 205118 (2004).
- ³⁶ E. H. Lieb, *Phys. Rev. Lett.* **62**, 1201 (1989).
- ³⁷ F. F. Assaad and I. F. Herbut, *Phys. Rev. X* **3**, 031010 (2013).
- ³⁸ F. Parisen Toldin, M. Hohenadler, F. F. Assaad, and I. F. Herbut, *Phys. Rev. B* **91**, 165108 (2015).
- ³⁹ Y. Otsuka, S. Yunoki, and S. Sorella, *Phys. Rev. X* **6**, 011029 (2016).
- ⁴⁰ M. M. Wolf, F. Verstraete, M. B. Hastings, and J. I. Cirac, *Phys. Rev. Lett.* **100**, 070502 (2008).
- ⁴¹ S. Furukawa, V. Pasquier, and J. Shiraishi, *Phys. Rev. Lett.* **102**, 170602 (2009).
- ⁴² G. Barcza, R. M. Noack, J. Sólyom, and Ö. Legeza, *Phys. Rev. B* **92**, 125140 (2015).
- ⁴³ Ö. Legeza and J. Sólyom, *Phys. Rev. B* **68**, 195116 (2003).
- ⁴⁴ G. Vidal, J. I. Latorre, E. Rico, and A. Kitaev, *Phys. Rev. Lett.* **90**, 227902 (2003).
- ⁴⁵ P. Calabrese and J. Cardy, *J. Stat. Mech.* **2004**, P06002 (2004).
- ⁴⁶ Ö. Legeza and J. Sólyom, *Phys. Rev. Lett.* **96**, 116401 (2006).
- ⁴⁷ J. Rissler, R. M. Noack, and S. R. White, *Chem. Phys.* **323**, 519 (2006).
- ⁴⁸ L. Amico, R. Fazio, A. Osterloh, and V. Vedral, *Rev. Mod. Phys.* **80**, 517 (2008).
- ⁴⁹ Ö. Legeza and J. Sólyom, *Phys. Rev. B* **70**, 205118 (2004).
- ⁵⁰ T. O. Wehling, E. Şaşıoğlu, C. Friedrich, A. I. Lichtenstein, M. I. Katsnelson, and S. Blügel, *Phys. Rev. Lett.* **106**, 236805 (2011).
- ⁵¹ N. Kharche and V. Meunier, *J. Phys. Chem. Lett.* **7**, 1526 (2016).
- ⁵² S. Sorella and E. Tosatti, *EPL (Europhysics Letters)* **19**, 699 (1992).